Inorg. Chem. **2008**, *47*, 7377−7388

Ligand Field Stabilization and Activation Energies Revisited: Molecular Modeling of the Thermodynamic and Kinetic Properties of Divalent, First-Row Aqua Complexes

Robert J. Deeth* and Kris Randell

Inorganic Computational Chemistry Group, Department of Chemistry, University of Warwick, Coventry CV4 7AL, U.K.

Received April 7, 2008

Ligand Field Molecular Mechanics (LFMM) parameters have been developed for the hexaaqua complexes of the divalent first row metals V^{2+} through to Zn^{2+}. The LFMM parameters provide an explicit description of the d electron stabilization energies and are tuned to reproduce both the experimental structures and the relative energetics of the hexaaqua complexes in aqueous solution plus Johnson and Nelson's data (*Inorg. Chem.*, **1995**, *34*, 5666−5671) for hypothetical complexes from which the ligand field stabilization energy has been removed. The LFMM calculations automatically reveal the typical, strong Jahn−Teller distortions of the d^4 Cr(II) and d^9 Cu(II) species plus the structurally smaller, but still energetically significant, distortions of the d^6 Fe(II) and d^7 Co(II) complexes. The latter are largely mediated via M−O π interactions which are explicitly treated in the LFMM method via the Angular Overlap Model $e_{\pi\perp}$ parameter which treats the π interactions perpendicular to the ligand plane. Without further parameter modification, we then predict approximate reaction barriers for both associative and dissociative ligand exchange based on simplified model pathways. The correlation between computed barrier heights and experimental exchange rate constants is generally excellent with the slowest reactions (involving V and Ni) having the largest barriers while the fastest reactions (Cu and Cr) have near zero barriers. In agreement with experiment, the LFMM model further confirms that k(V) < k(Ni) and k(Co) < k(Fe) which contrasts with the classical crystal field activation energy analysis of Basolo and Pearson which predicts k(V) = k(Ni) and the reverse order of reactivity for Fe and Co species. LFMM further predicts a mechanistic changeover from an associatively activated process at Mn to dissociatively activated exchange for Fe, Co, and Ni which is consistent with experimental activation volumes and previously published high level quantum chemical calculations.

Introduction

Aquated metal ions are fundamental to transition metal (TM) chemistry. Hence, an enormous amount of experimental and theoretical research has been devoted to studying their structures, energetics, and dynamic behavior from both classical coordination chemistry and bioinorganic perspectives.[1–3]

A distinguishing feature of TM centers is an open d shell in at least one common oxidation state which can have a profound influence on the properties of the complex. For example, instead of a smooth variation from d^0 to d^{10} configurations, the experimental hydration enthalpies, ΔH_{hyd}, of the divalent ions Ca^{2+} through to Zn^{2+} exhibit the classical "double hump" behavior typical of first-row TM species. These variations correlate with the magnitude of the d orbital splitting and the concomitant ligand field stabilization energy (LFSE).

Qualitatively, the LFSE concept is well-known from elementary undergraduate courses in coordination chemistry. It depends on the formal d configuration and the spin state. More recently, Johnson and Nelson have made an extensive quantitative analysis of LFSEs for several types of complexes,[4–7] including the high spin (HS) divalent aqua ions.[5]

* To whom correspondence should be addressed. E-mail: r.j.deeth@warwick.ac.uk.

(1) Richens, D. T. *The Chemistry of Aqua Ions*; John Wiley & Sons: New York, 1997.
(2) Helm, L.; Merbach, A. E. *Coord. Chem. Rev.* **1999**, *187*, 151–181.
(3) Helm, L.; Merbach, A. E. *Chem. Rev.* **2005**, *105*, 1923–1959.
(4) Johnson, D. A.; Nelson, P. G. *J. Chem. Soc., Dalton Trans.* **1995**, 3483–3488.

10.1021/ic800628j CCC: $40.75
Published on Web 07/25/2008

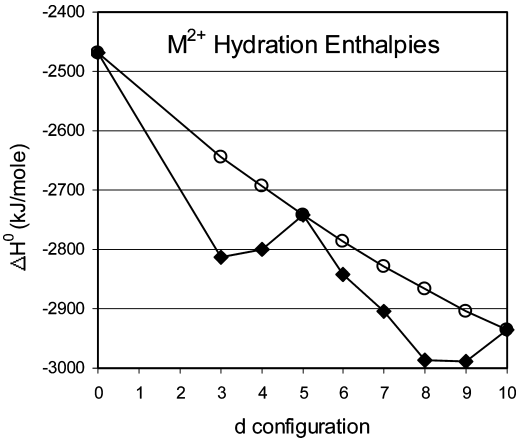

Figure 1. Experimental hydration enthalpies, ΔH^0, for first-row divalent metal ions Ca^{2+} through Zn^{2+} (solid diamonds) and the residual values, ΔH, which have been corrected for LFSE (open circles). Adapted from Johnson and Nelson.[5]

Table 1. Rate Constants for Water Exchange at Selected M^{2+} Centers

metal ion	k/s^{-1}[a]
V^{2+}	8.7×10^1
Cr^{2+}	2×10^9
Mn^{2+}	2.1×10^7
Fe^{2+}	4.4×10^6
Co^{2+}	3.2×10^6
Ni^{2+}	3.2×10^4
Cu^{2+}	4.4×10^9
Zn^{2+}	3×10^7

[a] All rate constants are expressed as first order rate constants for even though some processes are associative. See Figure 1 of ref 8.

Four contributions are identified—an orbital term, ΔE_{orb}, which depends on the octahedral splitting parameter Δ_{oct}, a correction based on interelectronic repulsion, ΔE_{rep}(irreg), a relaxation term, ΔE_{rlx}, describing the energy change as the M−O bond length relaxes from its (hypothetical) value in the absence of any LFSE to its actual value, and finally, a term related to spin−orbit coupling, ΔE_{so}.

Values for these terms were estimated independently and their sum subtracted from the experimental hydration enthalpy to yield residual hydration enthalpies, ΔH. As shown in Figure 1, the latter form a smooth line connecting the systems where the LFSE is formally zero, that is, d^0, high-spin d^5 and d^{10}.

The ground-state thermodynamic properties of first-row TM complexes are thus strongly influenced by the d electrons. Similarly, kinetic properties depend on the disposition of the d electrons. For example, the rate constants for solvent exchange, probably the simplest reaction for an aquated metal ion, can be correlated with d electron effects.

Water exchange rates (Table 1) span many orders of magnitude from extremely fast, for example, $k \sim 10^9$ s^{-1} for Cu^{2+} and Cr^{2+}, to extremely slow, for example, $k \sim 10^{-11}$ for Ir^{3+}.[8]

In the now-classical text book, Basolo and Pearson[9] used simple crystal field theory (CFT) to estimate the change in stabilization energy for a general exchange/substitution reaction. They considered both an associative process, with the (approximate) transition state (TS) modeled as a pentagonal bipyramid, and a dissociative process, with the TS modeled as a square pyramid, and computed the change as a function of the CFT parameter Dq ($\Delta_{oct} = 10Dq$). Although crude, the model is qualitatively successful and predicts for octahedral systems that, irrespective of the mechanism, d^3 and HS d^8reactions should be the slowest and HS d^4 and d^9 processes the fastest. For the remaining HS configurations, the model predicts the relative rates to be $d^5 < d^{1,6} < d^{2,7}$ for a dissociative process and $d^5 < d^{2,7} < d^{1,6}$ for an associative process.

While the predictions for the particular case of HS first-row hexaaqua M^{2+} complexes are thus (largely) qualitatively correct, the simple model has limitations. For example, by construction, we get exactly the same change for d^n and d^{n+5} configurations. Hence, the model predicts that both $[V(OH_2)_6]^{2+}$ and $[Ni(OH_2)_6]^{2+}$ should proceed via the same pathway and that it should be associative since this corresponds to a smaller stabilization energy change of −1.81Dq versus −2.0Dq for the dissociative route. This is inconsistent with experimental activation volume data which suggest a changeover in mechanism.

Activation volumes, $\Delta V^{\ddagger}$, derived from variable pressure NMR experiments change sign from negative on the left of the series (e.g., -4.1 cm^3 mol^{-1} for V) to positive on the right ($+7.2$ cm^3 mol^{-1} for Ni) suggesting the former is associative while the latter is dissociative.[2] The absence of observable intermediates implies an interchange (I) process with $[V(OH_2)_6]^{2+}$ reacting via an I_a mechanism while $[Ni(OH_2)_6]^{2+}$ goes via an I_d mechanism. Water exchange has also been studied theoretically. Åkesson et al.[10] suggested a uniformly dissociative mechanism, a claim which was later refuted by Rotzinger, again based on theoretical calculations.[11–14] The latter author states that while a dissociative process is always feasible and becomes progressively dominant with increasing numbers of d electrons, it is not necessarily favorable on the left side of the transition series. In particular, quantum chemical calculations for the vanadium species give the same activation parameters for both I_a and I_d whereupon the "best" mechanism is that which also rationalizes the experimental activation volume, in this case, I_a.

We are interested in modeling the ligand field contributions to the thermodynamic and kinetic properties of these simple hexaaqua complexes. The quantum mechanical calculations mentioned above implicitly treat the LFSE but are relatively compute intensive. In contrast, classical molecular mechanics (MM) is many orders of magnitude faster. However, given the important role of d electrons, any MM scheme must also

(5) Johnson, D. A.; Nelson, P. G. *Inorg. Chem.* **1995**, *34*, 5666–5671.
(6) Johnson, D. A.; Nelson, P. G. *Inorg. Chem.* **1995**, *34*, 3253–3259.
(7) Johnson, D. A.; Nelson, P. G. *Inorg. Chem.* **1999**, *38*, 4949–4955.
(8) Cusanelli, A.; Frey, U.; Richens, D. T.; Merbach, A. E. *J. Am. Chem. Soc.* **1996**, *118*, 5265–5271.
(9) Basolo, F.; Pearson, R. G. *Mechanisms of Inorganic Reactions*; John Wiley & Sons Inc: New York, 1967.
(10) Akesson, R.; Pettersson, L. G. M.; Sandstrom, M.; Wahlgren, U. *J. Am. Chem. Soc.* **1994**, *116*, 8705–8713.
(11) Rotzinger, F. P. *J. Am. Chem. Soc.* **1996**, *118*, 6760–6766.
(12) Rotzinger, F. P. *J. Phys. Chem. B* **2005**, *109*, 1510–1527.
(13) Rotzinger, F. P. *Helv. Chim. Acta* **2000**, *83*, 3006–3020.
(14) Rotzinger, F. P. *J. Am. Chem. Soc.* **1997**, *119*, 5230–5238.

account for the LFSE. Our ligand field molecular mechanics (LFMM)[15] approach is an extension of the conventional MM formalism specifically designed for open-shell d^n systems.[16] We explicitly include the most significant effects arising from the d electrons via a generalized ligand field theory (LFT) calculation of the LFSE based on the angular overlap model (AOM).[17] Several recent studies[18–22] have shown that the method is capable of delivering structures and relative conformer energies in good agreement both with experiment and high-level density functional theory (DFT) calculations but at a small fraction of the computational cost of the latter.

The present paper extends the LFMM parametrization to hexaaqua species of V(II) through to Zn(II). This includes an explicit treatment of both metal−water σ and π interactions. In addition to structures, we also develop parameters which deliver absolute molecular energies (i.e., hydration enthalpies) and which allow us to model reaction mechanisms (e.g., exchange rate constants) which involve bond-making and/or bond-breaking. As described below, by designing the LFMM parameters on the basis of the "ground state" thermodynamics, the kinetics are simultaneously and implicitly accounted for.

Computational Details

All LFMM calculations were carried out using DommiMOE,[23] our extended version of the Molecular Operating Environment, based on MOE2006.[24]

DFT calculations used the 2006 version of the Amsterdam density functional (ADF) program.[25] Geometry optimizations employed spin-unrestricted functionals as detailed in the text with basis sets of triple-ζ plus polarization (TZP) quality on the metal and double-ζ plus polarization (DZP) on all other atoms together with the frozen core approximation[26] (1s-2p on the metal and 1s on O). Default SCF and geometry convergence criteria were employed throughout.

Solvation effects were included via the Conductor-Like Screening Model (COSMO)[27–29] as implemented in ADF using radii derived from Allinger's MM3 force field. Natural Atomic Orbital (NAO) charges were obtained using NBO version 4 supplied with Jaguar 3.5[30] with the B3LYP functional and 6−31G* basis sets.

Table 2. Average Experimental and DFT-optimized M−O Bond Lengths (Å) for $[M(OH_2)_6]^{2+a}$

M	exp[b]	LDA	PW91	BLYP	RPBE
V	2.13	2.061	2.124	2.151	2.156
Cr	2.17	2.082	2.148	2.172	2.183
Mn	2.18	2.110	2.174	2.191	2.210
Fe	2.13	2.058	2.123	2.145	2.160
Co	2.09	2.018	2.084	2.105	2.118
Ni	2.06	1.985	2.053	2.074	2.085
Cu	2.09	2.009	2.075	2.098	2.109
Zn	2.10	2.034	2.093	2.112	2.132

[a] The DFT symmetry was effectively T_h although the actual computations used D_{2h} point symmetry. The effect of solvent was included via the COSMO model. [b] From ref 5.

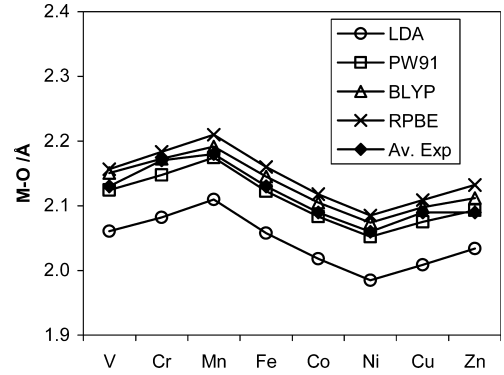

Figure 2. Comparison of the calculated metal−oxygen bond lengths with experimental values.

Results and Discussion

Johnson and Nelson[5] provide a detailed breakdown of the experimental structures and energies of $[M(OH_2)_6]^{2+}$ species into their component parts, ideally suited to the present study. However, at various points, we wish to augment experiment with data for hypothetical species where we will turn to DFT to provide the "missing" data. Consequently, we begin by using DFT to establish reliable computational protocols for modeling hexaaqua complexes. We acknowledge that we are by no means the first to report such results and that other methods have been tried and tested.[12] Our goal is not to explore the accuracy of DFT (or any other quantum approach) but rather to arrive at an internally validated form of DFT to assist with parametrizing the LFMM.

Initially, the average M−O bond lengths for a number of functionals were compared to the experimental estimates of Johnson and Nelson.[5] The ADF optimizations employed D_{2h} symmetry with all M−O distances constrained to the same (optimized) value. Although the true symmetry would therefore be T_h, this point group is not implemented in ADF. The averaged experimental data and the results for four common functionals LDA, PW91, BLYP, and RPBE are collected in Table 2 and compared graphically in Figure 2. With the chosen symmetry, the Cr, Fe, Co, and Cu systems

(15) Deeth, R. J. *Coord. Chem. Rev.* **2001**, *212*, 11–34.
(16) Burton, V. J.; Deeth, R. J.; Kemp, C. M.; Gilbert, P. J. *J. Am. Chem. Soc.* **1995**, *117*, 8407–8415.
(17) Schaeffer, C. E.; Jorgensen, C. K. *Mol. Phys.* **1965**, *9*, 401.
(18) Deeth, R. J. *Inorg. Chem.* **2007**, *46*, 4492–4503.
(19) Deeth, R. J.; Hearnshaw, L. J. A. *Dalton Trans.* **2006**, 1092–1100.
(20) Deeth, R. J. *Chem. Commun.* **2006**, 2551–2553.
(21) Lautru, S.; Deeth, R. J.; Bailey, L. M.; Challis, G. L. *Nature Chem. Biol.* **2005**, *1*, 265–269.
(22) Deeth, R. J.; Hearnshaw, L. J. A. *Dalton Trans.* **2005**, 3638–3645.
(23) Deeth, R. J.; Fey, N.; Williams-Hubbard, B. J. *J. Comput. Chem.* **2005**, *26*, 123–130.
(24) MOE *Molecular Operating Environment*, 2006.06; Chemical Computing Group, Montreal: Montreal, 2006.
(25) Baerends, E. J.; Bérces, A.; Bo, C.; Boerrigter, P. M.; Cavallo, L.; Deng, L.; Dickson, R. M.; Ellis, D. E.; Fan, L.; Fischer, T. H.; Fonseca Guerra, C.; van Gisbergen, S. J. A.; Groeneveld, J. A.; Gritsenko, O. V.; Harris, F. E.; van den Hoek, P.; Jacobsen, H.; van Kessel, G.; Kootstra, F.; van Lenthe, E.; Osinga, V. P.; Philipsen, P. H. T.; Post, D.; Pye, C. C.; Ravenek, W.; Ros, P.; Schipper, P. R. T.; Schreckenbach, G.; Snijders, J. G.; Sola, M.; Swerhone, D.; te Velde, G.; Vernooijs, P.; Versluis, L.; Visser, O.; van Wezenbeek, E.; Wiesenekker, G.; Wolff, S. K.; Woo, T. K.; Ziegler, T. *ADF 2006.01*, Scientific Computing and Modelling NV, Free University, Amsterdam: Amsterdam, 2006.
(26) Baerends, E. J.; Ellis, D. E.; Ros, P. *Theoret. Chim. Acta* **1972**, *27*, 339.
(27) Klamt, A.; Schüürmann, G. *J. Chem. Soc., Perkin Trans.* **1993**, *2*, 799.
(28) Klamt, A. *J. Phys. Chem.* **1995**, *99*, 2224.
(29) Klamt, A.; Jones, V. *J. Chem. Phys.* **1996**, *105*, 9972.
(30) *Jaguar*, version 3.5; Schrodinger, Inc.: Portland, Oregon, 1998.

are formally Jahn−Teller active but in any event, none of the complexes is actually a local minimum. As described later, minor movements of the hydrogen atoms are required to generate true minima but these changes have no significant effect on the M−O distances.

All the functionals show the same trend. The LDA systematically underestimates the M−O distances, consistent with the normal view that the LDA leads to overbinding.[31] We note, however, that the influence of the solvation is an important factor in that the COSMO field reduces the gas-phase bond lengths by 0.02 to 0.04 Å. Thus, gas-phase LDA structures would accidentally appear in better agreement with experiment than those obtained using gradient corrected functionals.[32] We have recently discussed the importance of taking some account of environmental effects if, as here, computed structures of TM systems are to be reliably compared with condensed phase experimental data such as from single crystal X-ray diffraction or solution EXAFS studies.[33]

The gradient-corrected functionals are all in better agreement with the experimentally derived bond lengths than the LDA but there is little to choose between them. The small discrepancies at Cr and Cu are slight artifacts due to the way that the "experimental" data were derived for these strongly Jahn−Teller distorted systems. On balance, PW91 appears to perform the best, and this functional was therefore chosen to aid the LFMM parametrization.

The types of parameters required for LFMM have been described in detail before.[23] Briefly, we use the existing force field (FF) for everything except the metal and its immediately bonded neighbors. Thus, the "conventional" M−L stretching term and L−M−L angle bending term are replaced by our own M−L stretch based on a Morse curve, and an explicit L−L repulsion term to help define the angular geometry around the metal center.

The force constants for any torsional rotations around the M−L bonds are set to zero to avoid the problems associated with *trans*-related ligands, where three colinear atoms lead to undefined torsion terms, while the FF must be augmented by explicit M−L−A angle bend terms. We normally set the latter's force constants to low values. Nonbonded interactions are considered, as normal, for 1,4 interactions and beyond. Depending on the FF, the 1,4 interactions may be scaled by a factor less than one, for example, MMFF uses a scaling factor of 0.75. For $[M(OH_2)_6]^{2+}$ species, therefore, the "original" FF terms comprise the O−H stretch, the H−O−H bend, and the nonbonded terms, to which we add the M−O−H angle bend. The LFMM part handles the M−L stretch, the L−L repulsion, and, crucially, the d-electron stabilization energy.

The LFSE is captured via a generalized ligand field theory calculation based on the angular overlap model. In principle, water can act as a σ donor and a π donor (Figure 3). In D_{2h}

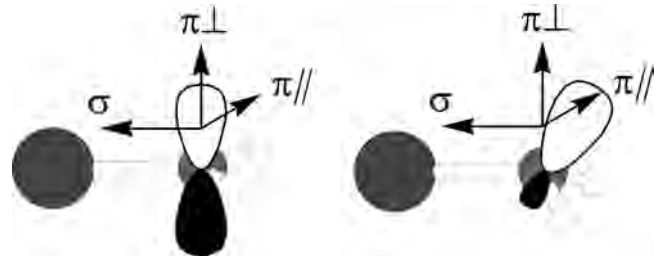

Figure 3. M−OH_2 coordination modes.

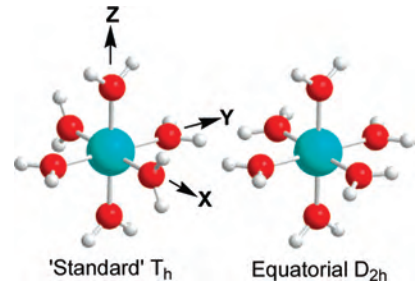

Figure 4. Ligand arrangements for $[M(OH_2)_6]^{2+}$ complexes. The "standard" geometry is of T_h symmetry which has D_{2h} as a possible subgroup.

symmetry, the ligand is 'trigonal' (i.e., sp^2 hybridized) such that the metal and OH_2 are coplanar. Hence, in the context of the AOM, a π interaction is expected only perpendicular to the M−OH_2 plane since the in-plane orbitals on the oxygen are used in O−H bond formation (Figure 3, left). Indeed, even if the water molecules tilt ($\sim sp^3$ hybridized), no "in-plane" interactions are expected (Figure 3, right). Thus, bent-bonding notwithstanding,[34,35] only two AOM parameters, e_σ and $e_{\pi\perp}$, are required, and we use experimental data and DFT calculations to help define their values.

Our first problem is that, given the symmetry, independent values for two AOM parameters cannot be derived from the d-orbital splittings. The "standard" D_{2h} geometry (Figure 4, left) being actually T_h, a cubic group, results in the d-orbitals splitting into one doubly and one triply degenerate set, e_g and t_g in T_h, that is, only one degree of freedom remains. The presence of π bonding in just one direction alters the overall splitting, Δ_{oct}, such that $\Delta_{oct} = 3e_\sigma - 2e_{\pi\perp}$ as opposed to $\Delta_{oct} = 3e_\sigma - 4e_\pi$ for a true octahedron, where the ligand would have to engage in cylindrically symmetric π bonding with $e_{\pi x} = e_{\pi y}$.

To circumvent this problem, an alternative D_{2h} geometry was chosen by rotating the ligands on the X axis through 90 ° such that four "equatorial" water ligands lie in the XY plane (Figure 4, right).

Using this "equatorial" geometry, but with all M−O distances constrained as before, the degeneracy of the d_π orbitals, d_{xz}, d_{yz}, and d_{xy}, is raised such that, within the AOM formalism and using the axis frame shown in Figure 4, they have energies of $4e_{\pi\perp}$, $2e_{\pi\perp}$, and 0, respectively. An estimate of $e_{\pi\perp}$ can thus be obtained from the corresponding DFT orbital energies, that is, from the Kohn−Sham orbitals with the largest d_{xz}, d_{yz}, or d_{xy} contributions, obtained for complexes with orbitally nondegenerate ground states to mini-

(31) Vanleeuwen, R.; Baerends, E. J. *Int. J. Quantum Chem.* **1994**, *52*, 711–730.
(32) Bray, M. R.; Deeth, R. J.; Paget, V. J.; Sheen, P. D. *Int. J. Quantum Chem.* **1997**, *61*, 85–91.
(33) Hocking, R. K.; Deeth, R. J.; Hambley, T. W. *Inorg. Chem.* **2007**, *46*, 8238–8244.
(34) Deeth, R. J.; Gerloch, M. *Inorg. Chem.* **1987**, *26*, 2582–2585.
(35) Deeth, R. J.; Duer, M. J.; Gerloch, M. *Inorg. Chem.* **1987**, *26*, 2578–2582.

Table 3. MO Energies (eV) for Selected $[M(OH_2)_6]^{2+}$ Complexes Using the Averaged PW91 M−O Bond Lengths and the "equatorial" D_{2h} Geometry Shown in Figure 4[a]

	V	Mn	Ni
$E(d_{xz})$	−12.2209	−15.3144	−15.3964
	0.0	0.0	0.0
$E(d_{yz})$	−11.8343	−14.9348	−14.9772
	0.387 (3121)	0.380 (3065)	0.419 (3380)
$E(d_{xy})$	−11.5172	−14.6194	−14.6807
	0.704 (5678)	0.695 (5606)	0.716 (5775)

[a] For each entry, the actual MO energy is quoted on top and the energy relative to the lowest MO underneath with the corresponding value in cm^{-1} in parentheses.

mize artifacts arising from an asymmetrical d electron potential.[36]

Table 3 gives the absolute and relative energies of the d_{xz}, d_{yz}, and d_{xy} MOs. The relative splittings for $[V(OH_2)_6]^{2+}$ and $[Ni(OH_2)_6]^{2+}$ are remarkably similar especially given the rather different Δ_{oct} values of 12300 and 8500 cm^{-1} respectively. This suggests that, within the DFT picture, M−OH_2 π bonding does not vary significantly as a function of the metal. Irrespective of how the data are treated (the sum of the relative MO energies is $6e_{\pi\perp}$ or the average separation between successive MOs is $2e_{\pi\perp}$), $e_{\pi\perp}$ is 1480 ± 50 cm^{-1}.

Having established a numerical value for $e_{\pi\perp}$, e_σ could simply be adjusted to deliver the observed values of Δ_{oct}. However, as described below, some modification of this expectation is required. Meanwhile, we need to consider how the AOM parameters vary as a function of M−O bond length. In electrostatic CFT, Δ_{oct} depends on the inverse fifth power of the bond length.[37] The change in Δ_{oct} was computed for $[V(OH_2)_6]^{2+}$ and $[Ni(OH_2)_6]^{2+}$ using DFT, and the resulting values fitted to a single exponent curve (Figure 5). The exponents are 5.4 and 5.5 respectively, sufficiently close to the CFT value for us to use a $1/r^5$ dependence for both e_σ and $e_{\pi\perp}$. Note that this choice is not critical. Providing suitable adjustments are made in the other parameters, other power dependencies could be used.

For a completely general LFMM treatment, the d−s mixing AOM parameter, e_{ds}, is also required.[38,39] This term depends on the symmetry and, in tetragonal systems, describes the configuration interaction stabilization of the d_{z^2} orbital by the higher energy valence metal s function. In octahedral (and T_h) symmetry, its effect is rigorously zero and thus for V, Mn, Fe, Co, and Zn complexes where all six M−O bond lengths should be very similar, we expect e_{ds} to play only a minor role. However, it will be significant for the strongly Jahn−Teller-distorted Cr and Cu complexes. Previous experimental spectroscopic measurements on planar M^{II} systems suggest $e_{ds} \sim 1500$ cm^{-1} for oxygen, nitrogen, and chloride donors.[40]

As in previous applications to Cu^{2+} systems,[19] we assume a $1/r^6$ dependence for e_{ds}. The Jahn−Teller effect for octahedral systems with doubly orbitally degenerate ground states is a balance between three competing factors: the (anharmonic) vibrational potential, the (nonlinear) Jahn−Teller coupling energy, and the d−s mixing.[41] All three have roughly comparable magnitudes, but the first and third terms favor a tetragonal elongation while the second term favors compression. Hence, the first two terms cancel, and e_{ds} acts like a switch which, once it exceeds a certain threshold, causes the elongated geometry to be lower in energy than the compressed structure which is now a saddle point.[19] A secondary effect of e_{ds} is to vary the size of the Jahn−Teller distortion, and we will use this feature to refine its value as described below. Before that, we consider e_σ.

The values for e_σ are ultimately derived from the hydration enthalpies. First, ΔH_{hyd}, is separated into the internal energy of $[M(OH_2)_6]^{2+}$, U_t, plus the solvation energy, U_{sol}, such that $\Delta H_{hyd} = U_t + U_{sol}$. The former is the "target" for the LFMM while the latter is estimated from the COSMO calculations. Of course, COSMO is designed to yield solvation free energies. However, it is known that the entropic contribution for metal ion hydration is small (∼2% of the free energy) plus whatever error we introduce will be similar for each complex and thus should effectively cancel out. We believe the COSMO "corrections" will be accurate enough.

The internal energy, U_t, is further subdivided into the LFSE and the residual internal energy, U_{res}. Following Johnson and Nelson, U_{res} corresponds to the interpolated points between those where the LFSE is formally zero, that is, d^0 Ca^{2+}, high-spin d^5 Mn^{2+}, and d^{10} Zn^{2+}. The relevant data are collected in Table 4 and include the numbers for calcium although this metal is not considered further.

We need to refine eight parameters, namely, the AOM e_σ and e_{ds} parameters, three Morse function parameters (D, r_0, α), the ligand−ligand repulsion parameter, A_{LL}, and the two partial atomic charges, ρ(O) and ρ(H). To reduce the number of variables, we begin by exploring whether partial atomic charges can be derived independently from quantum chemical calculations.

Mulliken charges (Mull) and natural atomic orbital (NAO) charges were computed for the Mn(II) and Zn(II) complexes since these complexes have orbitally nondegenerate ground states and the Jaguar program was able to employ the full T_h symmetry. In addition, we explored Jahn−Teller distorted $[Cu(OH_2)_6]^{2+}$ to see the effect of long and short metal−ligand distances on the charge distribution in the water ligands. The data are collected in Table 5.

The Mulliken charges have smaller magnitudes than the NAO charges suggesting a more covalent description than the other, more sophisticated charge partitioning scheme. However, in each case, the charges are remarkably constant providing the basis set is not changed. Hence, despite varying the Mn−O distance over 0.3 Å, the O and H charges change by only 0.01. Of course, all the small changes on the ligands result in a larger change on the metal (0.15) but given that this will be screened to some degree by the ligand atoms, the data in Table 5 suggest a single set of charges will suffice

(36) Deeth, R. J. *Faraday Discuss.* **2003**, *124*, 379–391.
(37) Bethe, H. A. *Ann. Physik.* **1929**, *3*, 133.
(38) Riley, M. J. *Inorg. Chim. Acta* **1998**, *268*, 55–62.
(39) Smith, D. W. *Inorg. Chim. Acta* **1977**, *22*, 107.
(40) Hitchman, M. A.; Cassidy, P. J. *Inorg. Chem.* **1979**, *18*, 1745.
(41) Deeth, R. J.; Hitchman, M. A. *Inorg. Chem.* **1986**, *25*, 1225–1233.
(42) Griffiths, J. S. *The Theory of Transition-Metal Ions*, 1st ed.; Cambridge University Press: Cambridge, 1961.

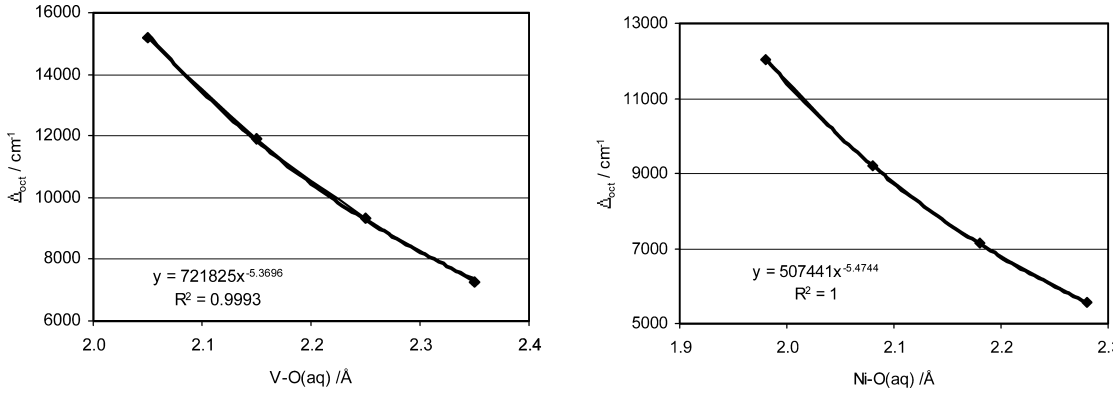

Figure 5. Power dependence of calculated Δ_{oct} values (cm^{-1}) as a function of M−O distance (Å).

Table 4. Experimental Hydration Enthalpies, COSMO Solvation Energies (D_{2h} Symmetry), and Target Internal Energies, U_t, for $[M(OH_2)_6]^{2+}$ Complexes[a]

metal	ΔH_{hydr}	E(COSMO)	U_{res}	LFSE	U_t
Ca	−377	−203	−174	0	−174
V	−458	−207	−211	−40	−251
Cr	−455	−207	−222	−25	−247
Mn	−440	−206	−233	0	−233
Fe	−465	−208	−244	−13	−256
Co	−477	−209	−254	−17	−268
Ni	−503	−210	−264	−29	−293
Cu	−502	−209	−273	−20	−293
Zn	−489	−207	−282	0	−282

[a] All data in kcal mol^{-1}.

Table 5. Calculated Partial Atomic Charges, ρ, for Various $[M(OH_2)_6]^{2+}$ Complexes With Various M−O Distances[a]

Metal: M−O/Å	ρ(M) Mull; NAO	ρ(O) Mull; NAO	ρ(H) Mull; NAO
Mn: 2.104#	1.05; 1.53	−0.81; −1.01	0.48; 0.55
Mn: 2.204	1.02; 1.60	−0.81; −1.02	0.49; 0.54
Mn: 2.193 (aq)	0.98; 1.58	−0.82; −1.03	0.50; 0.55
Mn: 2.404#	0.99; 1.68	−0.80; −1.02	0.49; 0.54
Zn: 2.133	1.13; 1.68	−0.83; −1.03	0.49; 0.54
Zn: 2.158 6-31+G*	1.33; 1.75	−1.00; −1.08	0.56; 0.56
Cu: 2.256 Å		−0.79; −1.02	0.47; 0.53
2.023 Å	0.86; 1.53	−0.78; −1.01	0.50; 0.55
2.028 Å		−0.79; −1.01	0.50; 0.55
water		−0.77; −0.93	0.39; 0.47
water (aq)		−0.88; −1.01	0.44; 0.51

[a] # Indicates M−O distance fixed at the stated value, otherwise the molecule was fully optimized either in the gas phase or using a continuum solvation treatment for aqueous solution (aq). Mull = Mulliken Populations; NAO = Natural Atomic Orbital Charges. The 6-31G* basis set was used (LACVP* for the metals) unless otherwise stated. Data for a single water molecule are included for comparison.

for all the aqua ions considered here. Given the well-known vagaries of Mulliken charges, it is tempting to focus on the NAO scheme. However, we ended up introducing a third "intermediate" set of charges in response to the comparison between LFMM and DFT geometries.

The DFT vibrational energies for D_{2h}-symmetric systems include several imaginary frequencies. This behavior has been noted before[11,14] but no further analysis appears to have been attempted. Animation of the imaginary modes revealed hydrogen atom movements which we used to obtain optimized geometries with no imaginary modes. These true local minima do not significantly differ in either the total energies or the M−O distances from the D_{2h} precursor but there are subtle alterations in the ligand orientations (Figure 6). The planes of the water pitch forward to expose the "back" of

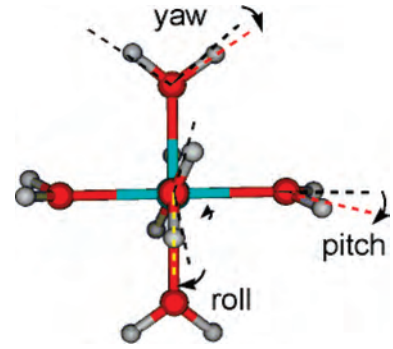

Figure 6. Deviations from "ideal" trigonal planar water orientation.

Table 6. Partial Atomic Charge Schemes

scheme	ρ(M)	ρ(O)	ρ(H)
natural	1.64	−1.02	0.54
intermediate	1.40	−0.82	0.46
Mulliken	1.22	−0.55	0.34

the oxygen to the H atom of an adjacent ligand to form a weak internal hydrogen bond. This H atom in turn rolls about the M−O direction such that its O−H vector aligns with the M−O vector of the ligand with which it forms the internal H-bond. Finally, there is a very small yawing motion such that the M−O−H angle for the H which points to the back of an adjacent O atom is slightly smaller than the M−O−H angle for the H atom that points away from the complex.

These subtle but distinctive structural changes have implications for the LFMM charges. The MMFF scheme enables 75% scaled 1−4 and full 1−5 electrostatic interactions. For the aqua complexes, this translates to attractive 1−4 O−H interactions and repulsive 1−5 H−H interactions. However, the Mulliken charges are not large enough to induce tilting and the LFMM structures retain trigonal water coordination. Natural charges reproduce the tilting quite well but the resulting electrostatic energies are alarmingly large. Consequently, we use a third set of charges sufficiently large in magnitude to induce tilting without generating overly dominant electrostatic energies.

Having fixed the partial atomic charges (Table 6), the remaining parameters are determined as follows. The ligand−ligand repulsion parameter, A_{LL}, was correlated with the "spherical" DFT interaction energy, E_{sph}, computed between a bare, spherical M^{2+} ion and six water molecules at their "in-complex" positions, that is, at r_{sph}, which is the

bond length in the absence of the LFSE as estimated by Johnson and Nelson. E_{sph} becomes progressively more negative from V^{2+} to Cu^{2+} and then increases at Zn^{2+} thus paralleling the Irving−Williams series. An increasingly negative contribution to the total energy can be achieved in many ways. We could progressively increase D or progressively decrease A_{LL}. We took the latter route with A_{LL} for $[V(OH_2)_6]^{2+}$ assigned a value of 5350 kcal mol^{-1} Å^{-6} decreasing linearly to 5000 kcal mol^{-1} Å^{-6} at Zn^{2+}. Of course, these values are not unique but they do provide a "background" against which the other parameters may be optimized. Other combinations were tried but the fitting process effectively ensures the same final result. However, it does mean that we should not confer particular significance to any single parameter.

There remain five parameters, e_σ, e_{ds}, D, α, and r_0, and we have four pieces of information, U_t, U_{res}, r_{oct}, and r_{sph}. In addition, therefore, we also computed the symmetric stretching frequency, ν_s, for the orbitally nondegenerate complexes. These data are included in our fitting set.

If all the ligands are equivalent, the highest point symmetry of our complexes is now S_6. However, to aid subsequent discussion, we will use the lower C_i symmetry as this will enable us to describe all the geometries in a unified way. For C_i structures, there will be three pairs of centrosymmetrically related ligands at distances r1, r2 and r3. Starting with the nondegenerate (S_6) systems (V^{2+}, Mn^{2+}, Ni^{2+} and Zn^{2+}), we take a guess at α and then adjust D and r_0 to reproduce U_{res} and r_{sph} in the absence of any ligand field contributions. Then e_σ is varied until the total LFMM energy is U_t. Hence, the target energy will be largely, but not exclusively, determined by the electronic energy term since there will be contributions from the other FF terms because of the change in geometry.

The optimized M−O bond length is compared to r_{oct}, and the symmetric stretching frequencies compare. The tolerances are ± 0.01 Å for distances and ± 10% for vibrations. If necessary, α is adjusted and the process repeated. For the strongly Jahn−Teller distorted systems (C_i), both e_{ds} and e_σ are varied to get the best agreement with the DFT structure while retaining the constraint that the total LFMM energy remains equal to U_t. An e_{ds} a_6 parameter value of 300 000 kcal mol^{-1} Å^{-6} works well for both Cr^{2+} and Cu^{2+} and is used for all systems. The parameters for Fe^{2+} and Co^{2+} are derived in a similar way except the tolerance for the structural comparisons is increased because of the π-type Jahn−Teller distortions (vide infra). The comparison of LFMM and target data for the intermediate charge set is given in Table 7 and LFMM parameter values in Table 8.

The LFMM parameters are designed to reproduce the target energetic data (U_t and U_{res}) for hexaaqua complexes plus their respective M−O bond lengths. Why then are the "effective" Δ_{oct} values obtained from fitting the energetic data (column Δ_{oct}(fit) in Table 8) close, but not identical to, the spectroscopic Δ_{oct} values? We are expecting problems for the obviously Jahn−Teller active Cu^{2+} and Cr^{2+} systems since the experimental data cannot be interpreted within octahedral symmetry. In contrast, the d−d spectra of $[Fe(OH_2)_6]^{2+}$ and $[Co(OH_2)_6]^{2+}$ are readily analyzed assuming octahedral symmetry yet the "experimental" Δ_{oct} values are quite different to those based on the LFMM D_{2h} model. However, here too, Jahn−Teller distortions confuse the interpretation of the spectra.

For example, $[Fe(OH_2)_6]^{2+}$ has an experimental Δ_{oct} value of 9400 to 10 400 cm^{-1}, depending on the data source (refs 5 and 42 respectively), which translates to an LFSE of between −11 and −13 kcal mol^{-1} while the LFMM treatment for a "symmetric" D_{2h} system with a bond length of ∼2.13 Å implies $e_\sigma \sim 2700$ cm^{-1} giving a Δ_{oct} value of only 5200 cm^{-1} and an apparent LFSE of only ∼6 kcal mol^{-1}. However, the fully optimized (i.e., Jahn−Teller distorted) $[Fe(OH_2)_6]^{2+}$ complex is not symmetric D_{2h} and the computed d-orbital energies for the "true" geometry span about 8000 cm^{-1}. However, the LFMM parameters were not fitted to the spectroscopic Δ_{oct} values but rather to the energy change from a "spherical" configuration complex, where the LFSE is zero, to the true system—a change of −13 kcal mol^{-1}. In fact, with the current parameters, the electronic contribution is actually slightly more negative at −13.5 kcal mol^{-1}. However, the geometry change also affects the other FF terms with the ligand−ligand repulsion increasing by 6 kcal mol^{-1} (the bonds are shorter on average) while the

Table 7. Comparison of DFT (Underlined), Johnson−Nelson (Bold) and LFMM (Italics) Data for Intermediate Charge Set

			r_{min}			
metal	r_{sph}	r_{oct}^{JN}	r1	r2	r3	ν_s (a_1)/cm^{-1}
V	2.20			2.14		335
	2.235	**2.137**				
	2.21			*2.13*		*352*
Cr	2.18		2.08	2.07	2.41	
	2.205	**2.167**				
	2.24		*2.08*	*2.08*	*2.37*	
Mn	2.18			2.18		332
	2.178	**2.178**				
	2.18			*2.18*		*337*
Fe	2.14		2.12	2.15	2.13	
	2.155	**2.126**				
	2.15		*2.12*	*2.12*	*2.12*	
Co	2.13		2.12	2.09	2.11	
	2.135	**2.093**				
	2.14		*2.05*	*2.05*	*2.14*	
Ni	2.12			2.08		347
	2.119	**2.060**				
	2.13			*2.08*		*353*
Cu	2.12		2.02	2.02	2.32	
	2.106	**2.087**				
	2.13		*1.97*	*1.97*	*2.31*	
Zn	2.12			2.12		328
	2.097	**2.097**				
	2.13			*2.13*		*363*

Table 8. LFMM Parameters and Derived Δ_{oct} Values[a]

metal	D	r_0	α	A_{LL}	$a_5(e_\sigma)^b$	$a_5(e_{\pi\perp})$	Δ_{oct}(fit)	Δ_{oct}(exp)[b]
V	22.3	2.13	1.60	5350	228000	60500	13024	12300[c], 12400
Cr	23.5	2.19	1.50	5300	263000	64000	14455	9250[c], 14000[d]
Mn	26.4	2.08	1.70	5250				8300
Fe	28.6	2.04	1.70	5200	115000	60300	5203	9350[c], 10400
Co	30.8	2.00	1.70	5150	105000	55000	5125	8400[c], 9300
Ni	32.0	2.02	1.60	5100	150000	51000	9542	8600[c], 8500
Cu	33.9	1.97	1.40	5050	161000	53900	9754	7850[c], 13000[d]
Zn	37.5	1.93	1.50	5000				

[a] $a_6(e_{ds}) = 300\,000$ kcal mol^{-1} Å^{-6}. [b] Griffiths, ref 42. [c] Johnson and Nelson, ref 5. [d] Value based on position of absorption maximum.

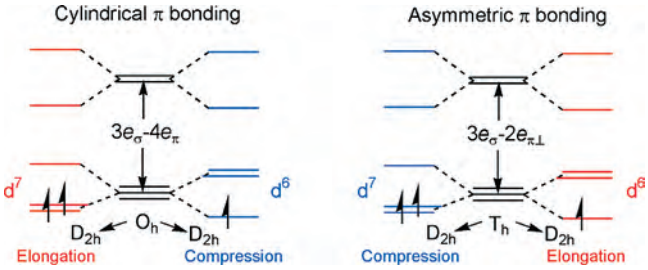

Figure 7. Constrained Jahn−Teller distortions for $[Fe(OH_2)_6]^{2+}$ and $[Co(OH_2)_6]^{2+}$.

Morse and electrostatic energies both decrease by about −5.5 kcal mol^{-1} in total. The combination of all the terms returns the required energy change of −13 kcal mol^{-1}.

The Jahn−Teller activity in $[Fe(OH_2)_6]^{2+}$ and $[Co(OH_2)_6]^{2+}$ deserves further study. Both have orbital triplet ground states (^5T_g and ^4T_g in T_h symmetry) which lead to very complicated T⊗ t vibronic coupling. For the purposes of analyzing the sense of any distortions, the problem can be simplified by restraining the symmetry to D_{2h}, that is, the degeneracy can only be raised via bond length alterations, and we can use simple arguments to predict whether the Jahn−Teller distortion will be a tetragonal elongation or a tetragonal compression. By ensuring that the LFMM calculation is also constrained to D_{2h} symmetry, we can then make a direct comparison between DFT and LFMM and thus verify that the LFMM behaves correctly.

Consider an octahedral system with cylindrically symmetric π interactions, that is, $e_{\pi x} \equiv e_{\pi y}$. The AOM d_π energies are

$$E(d_{xy}) = 2e_\pi(x) + 2e_\pi(y) \quad (1a)$$

$$E(d_{xz}) = 2e_\pi(x) + 2e_\pi(z) \quad (1b)$$

$$E(d_{yz}) = 2e_\pi(y) + 2e_\pi(z) \quad (1c)$$

where x, y, and z refer to the Cartesian axes on which the ligands lie. For a tetragonal compression along the z axis and $e_\pi > 0$ (a π donor), $e_\pi(z) > e_\pi(x) = e_\pi(y)$ and hence $E(d_{xz}) = E(d_{yz}) > E(d_{xy})$. The reverse splitting pattern is obtained for a tetragonal elongation. Hence, to avoid generating a degenerate state, which would still be Jahn−Teller active, a d^6 configuration favors compression while the d^7 configuration favors elongation.

Next, consider water ligation ($e_{\pi\perp} > 0$) with the structure and axis frame definition shown on the left of Figure 4. Here, the d_π functions have energies

$$E(d_{xy}) = 2e_{\pi\perp}(x) \quad (2a)$$

$$E(d_{xz}) = 2e_{\pi\perp}(z) \quad (2b)$$

$$E(d_{yz}) = 2e_{\pi\perp}(y) \quad (2c)$$

In this case, the same tetragonal compression gives $E(d_{xz}) > E(d_{yz}) = E(d_{xy})$ and elongation gives $E(d_{xz}) = E(d_{yz}) > E(d_{xy})$, that is, the reverse sense to cylindrical π bonding, and thus the reverse sense of the Jahn−Teller distortion is expected. These arguments are shown schematically in Figure 7.

To compare like with like, the LFMM optimization must also be in D_{2h} symmetry. To achieve this, every hydrogen atom was restrained such that the H−O−M−O torsion angle was zero. Under these conditions, both DFT and LFMM give a tetragonally elongated d^6 $[Fe(OH_2)_6]^{2+}$ with four short equatorial bonds of 2.09 Å (DFT) versus 2.12 Å (LFMM) and two longer bonds at 2.17 Å (DFT) versus 2.19 Å (LFMM). In contrast, d^7 $[Co(OH_2)_6]^{2+}$ is compressed with the four longer equatorial bonds at 2.11 Å (DFT) versus 2.12 Å (LFMM) and two shorter axial contacts at 2.02 Å (DFT) versus 2.04 Å (LFMM).

Both LFMM and DFT give exactly the same sense and a very similar magnitude of Jahn−Teller distortion in these systems. Note that the distortions in these model calculations are driven by the energy changes of the d_{xz}, d_{yz}, and d_{xy} orbitals and are thus exclusively due to π bonding. The LFMM is unique among FF-based approaches to TM complexes in being able to capture these effects. Moreover, they carry significant energetic consequences. The DFT calculations show that the change from T_h (all M−O bond lengths the same) to D_{2h} symmetry (three pairs of potentially dissimilar bonds) is accompanied by an energy lowering of 3 to 4 kcal mol^{-1}. Interestingly, despite the much larger structural change for the σ-type Jahn−Teller systems ($[Cr(OH_2)_6]^{2+}$ and $[Cu(OH_2)_6]^{2+}$), the energy change is similar for both the π-type *and* the σ-type. Apparently, π-type Jahn−Teller effects are just as important as the more easily recognizable σ-type effects.

Water Exchange Mechanism. The LFMM force field has been designed around a number of readily observable and/or calculable properties of hexaaqua complexes and tested on isolated species. The parametrization process was essentially guaranteed success and given that both structural and energetic data were used in the fitting process, the hope is that these parameters will provide a sound basis for extension to mixed-ligand systems. Thus, in addition to getting the correct structures, as in previous LFMM studies, we can also try to compute the composition of mixtures of different molecules in solution. Currently, the best we might hope for is to get reasonable conformational energies of a single system. Meanwhile, let us consider what additional applications and insights the new FF may lead to for aqua complexes.

The seminal work of Basolo and Pearson[9] established a qualitative relationship between the rate constant for water exchange and the change in crystal-field activation energy. While the approximations they employed were crude, this observation suggests that a model such as the LFMM, which explicitly treats the "true" LFSE, might be able to model the exchange process more accurately.

Substitution processes in coordination chemistry are usually classified according to whether they are associative, A, dissociative, D, or interchange, I. The first two imply the formation of an observable intermediate of higher (A) or lower (D) coordination number than the starting material. Between these two extremes lie the interchange processes which may be associatively or dissociatively activated, I_a or I_d, respectively.

Conventional molecular mechanics is designed for conformational searching where the connectivity remains con-

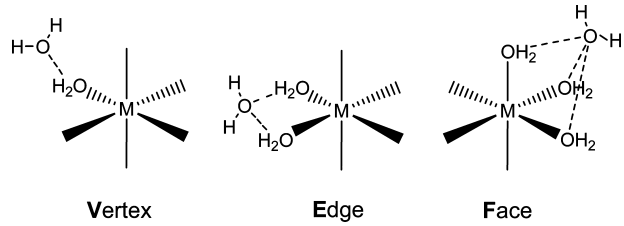

Figure 8. Schematic representations of the possible positions of a second coordination sphere water molecule interacting with bound water ligands at the vertex (V), edge (E), or face (F) of the octahedron.

stant. This does not mean that MM is incapable of treating bond-making and bond-breaking processes, including the intervening transition states, and several groups have proposed methods for modeling reaction pathways, for example, Warshel's empirical valence bond scheme,[43] Goddard's ReaxFF,[44] or Truhlar's multiconfiguration molecular mechanics (MCMM)[45] approaches all generate smooth potential energy surfaces connecting reactants and products. To our knowledge, none of these methods has been applied to water exchange at TM centers.

The alternative to MM is quantum mechanics (QM) which has the major advantages of (i) not requiring special parametrization and (ii) being capable of following reaction pathways and automatically locating transition states. However, compared to MM, QM is orders of magnitude slower, and this problem can be greatly exacerbated for open-shell TM systems which may demand very expensive methods.[12]

In contrast, LFMM has been shown to give comparable results to QM, at least for molecular structures and conformer energies.[18–20,22,46,47] For the present aqua complexes, we have not taken any special steps to ensure an accurate treatment of the transition state but given that the reaction involves making and breaking metal−oxygen bonds and since the LFMM FF terms employ functions chosen to allow for dissociation (in particular, the Morse function for M−L stretching), we proceed with a series of calculations similar to what might be considered if full QM were being used.

The reference point for the reactant is $[M(OH_2)_6]^{2+}.H_2O$, that is, a hexaaqua ion with a seventh water in the second hydration shell. QM indicates three possible positions for the seventh water molecule which can interact with one, two, or three ligands as shown in Figure 8.

Previous calculations for both **V** and **E** forms for vanadium, manganese, and iron species have been reported using the PCM model for solvation effects,[13] and the edge form is found to be slightly lower than the vertex form. We have repeated the calculations for V and Mn and added those for Ni to provide an internally comparable set which also considers the facial isomer. DFT (PW91 plus COSMO solvation) consistently predicts the edge isomer, **E**, to be the most stable although there is not a big difference between **E** and **V** (Table 9). Our results are therefore consistent with the previous work.

Table 9. Relative Energies (kcal mol^{-1}) Computed via DFT (PW91) With COSMO Solvation Corrections of the Structures Shown in Figure 8

metal	E_{rel}(**V**)	E_{rel}(**E**)	E_{rel}(**F**)
V	0.5	0.0	2.5
Mn	1.1	0.0	2.8
Ni	0.6	0.0	1.9

The LFMM also places the extra water molecule between two coordinated ligands, that is, the **E** isomer. Neither the **V** nor the **F** forms appear to be local minima on the LFMM PE surfaces. The LFMM and DFT geometries are not significantly different.

However, what is far more significant is that the LFMM structure is not significantly perturbed when the additional water molecule is *explicitly connected* to the metal ion to give a formally seven-coordinate species which we will represent as $[M(OH_2)_6(OH_2)]^{2+}$ (Figure 9). The metal−oxygen distance for this uncoordinated group is 3.9−4 Å which would generate a severe energy penalty in conventional MM if the M−L stretch is represented by a quadratic or quartic expansion. The significance of the seventh water is that we need to retain the same number of M−O bonds for reactant and transition state. In particular, for an associative process, we need that explicit connection.

In the spirit of Basolo and Pearson's original work, our intent is not to provide a comprehensive analysis of all the possible solvent exchange mechanisms.[3] Rather, the simple model pathways we consider are as depicted in Figure 10. The associative model TS structure is relatively straightforward to locate manually since microscopic reversibility implies that the chemical environment of entering and leaving groups is the same. For V and Ni, this turns out to be a true first order saddle point (i.e., one negative frequency) while for the remaining complexes, it is a local minimum albeit in a very shallow well. The "TS" energy is always higher than the seven-coordinate starting point except for $[Cr(OH_2)_6(OH_2)]^{2+}$, for which the current parameter set gives a slightly lower energy than the edge-bound starting point.

Defining a suitable system to model the dissociative path is more problematic. Simply breaking a $M-OH_2$ bond in $[M(OH_2)_6]^{2+}$ and optimizing the resulting $\{[Ni(OH_2)_5]\cdot H_2O\}^{2+}$ is unsatisfactory since the number of M−O bonds in reactant and "transition state" are different. The second option is to retain six explicit bonds and simply reposition a water ligand to lie over an adjacent octahedral face. This procedure gave a local minimum for all $[M(OH_2)_6]^{2+}$ complexes except Mn^{2+} and Zn^{2+} where the system always collapsed back to "octahedral". The problem for Mn^{2+} was solved by moving a bound water ligand to lie over a face as before, thus keeping six explicit M−O bonds, but now retaining an additional, but explicitly disconnected, "dissociating" water molecule to give a complex of general formula $[M(OH_2)_5(OH_2)]^{2+}\cdot H_2O$. This leads to a "pseudo transition state", actually a local minimum, for all metals except Zn which again collapsed back to $[Zn(OH_2)_6]^{2+}\cdot H_2O$. It is not clear why zinc behaves differently in dissociative

(43) Warshel, A.; Weiss, R. M. *J. Am. Chem. Soc.* **1980**, *102*, 6218–6226.
(44) Nielson, K. D.; van Duin, A. C. T.; Oxgaard, J.; Deng, W. Q.; Goddard, W. A. *J. Phys. Chem. A* **2005**, *109*, 493–499.
(45) Albu, T. V.; Corchado, J. C.; Truhlar, D. G. *J. Phys. Chem. A* **2001**, *105*, 8465–8487.
(46) Diedrich, C.; Deeth, R. J. *Inorg. Chem.* **2008**, *47*, 2494–2506.
(47) Deeth, R. J.; Foulis, D. L.; Williams-Hubbard, B. J. *Dalton Trans.* **2003**, 3949–3955.

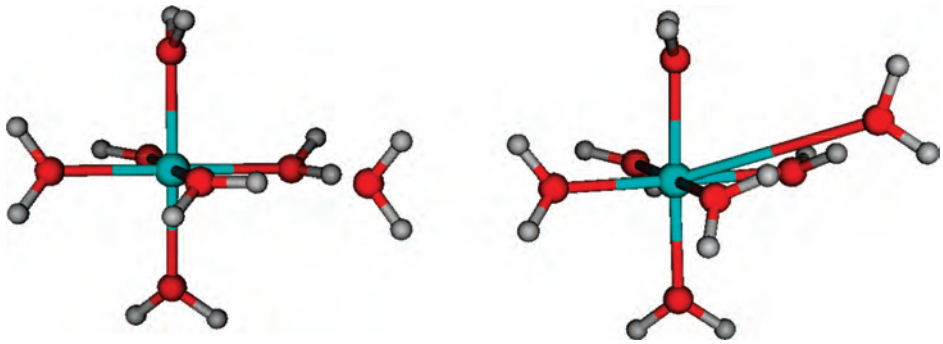

Figure 9. Effect of explicitly binding a seventh water ligand on LFMM geometry for $[V(OH_2)_6]^{2+}\cdot H_2O$.

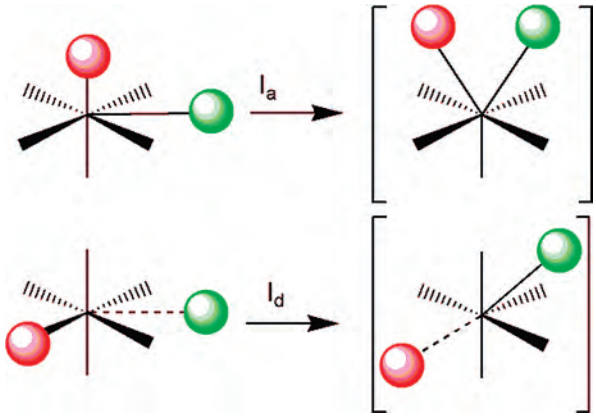

Figure 10. Schematic depiction of how the different reaction pathways were modeled. The green sphere represents the entering ligand while the red sphere is the leaving group. Solid lines represent explicit M−O bonds, dashed lines are for disconnected ligands.

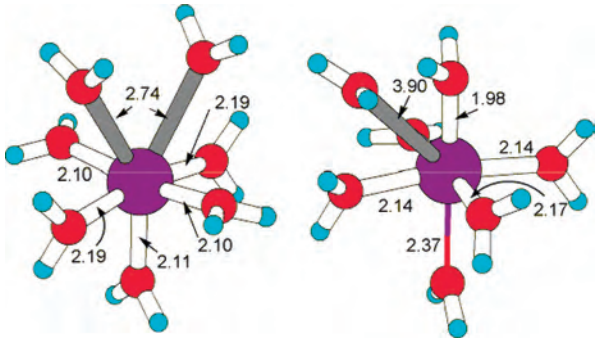

Figure 11. LFMM structures for vanadium complexes. Left: true TS for associative exchange. Right: approximate pseudo-TS for a simplified dissociative process. The "dissociated" ligand is represented by the red-purple colored connector and is not explicitly coordinated.

mode and pending further investigation, we omit this pathway for zinc from the following discussion. Meanwhile, using vanadium as an example, the LFMM structures for "associative" and "pseudodissociative" processes are shown in Figure 11.

The "activation energy" for associative activation is the difference in total LFMM energy between the seven-coordinate "ground" state (Figure 9, right) and the associative model "transition state" (Figure 11, left) while for dissociative activation, it is the difference between the energy of the pseudo-TS with six explicit M−O bonds, as illustrated for V on the right of Figure 11, and the $[M(OH_2)_6]^{2+}$ precursor. The Cr systems always gave a negative value: −1.3 kcal mol^{-1} for associative and −2.3 kcal mol^{-1} for

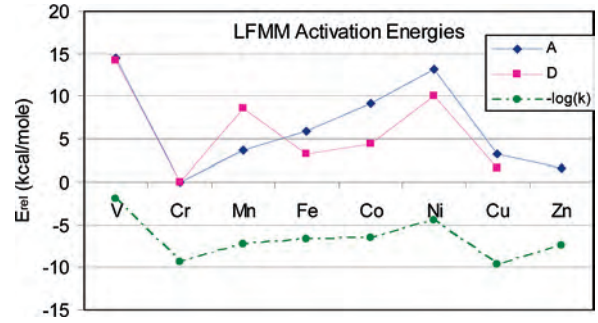

Figure 12. Calculated activation energies relative to Cr(II) compared to −log k, where k are the experimental exchange-rate constant. No suitable D pathway could be located for Zn which is therefore omitted from the graph.

dissociative. This is consistent with Cr having a fast exchange rate, but a negative activation energy does not seem physically reasonable. Consequently, and to aid the comparison, the computed activation energies were adjusted such the E_{act} for Cr is zero for both mechanistic pathways.

The resulting correlation between the experimental rate constants and the LFMM activation energies is surprisingly good. For example, we predict that associative and dissociative processes for vanadium(II) should have similar activation energies just as Rotzinger finds using high-level QM methods.[11,12] Moreover, not only are the general trends reproduced but the LFMM also predicts a mechanistic change from associative for V and Mn to dissociative for Fe, Co, and Ni, a feature which is consistent with the sign change in the volumes of activation.

The reactions at Cr and Cu are slightly ambiguous since the energies are not well separated so both mechanisms are predicted to be feasible. However, given the extreme elongation of the axial group in these strongly Jahn−Teller distorted systems, the distinction between associative and dissociative activation is blurred anyway. Zn is anomalous and behaves qualitatively differently from the open-shell systems. The dissociative process is expected to be more favorable than an associative one on the extreme right of the series but we cannot locate the same type of dissociative "TS" as for the other complexes, and the associative pathway for zinc is predicted to have a lower barrier than either of the copper pathways even though the experimental exchange rate is slower. The zinc species warrant further investigation.

For the other complexes, despite the many approximations, the qualitative predictions embodied in Figure 12 are reasonably robust. Modest variations in the LFMM

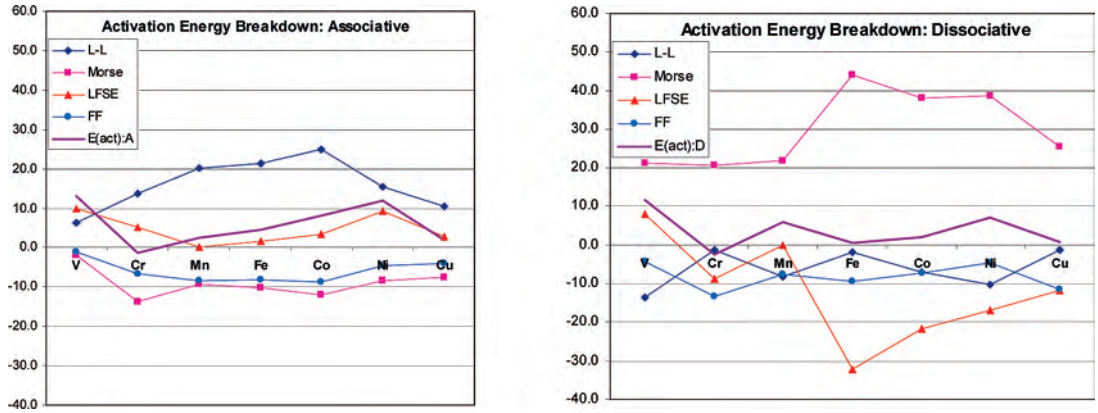

Figure 13. Breakdown of activation energies, *E*(act), into separate contributions from ligand−ligand repulsion (L−L), M−L bond stretching (Morse), LFSE, and any remaining FF terms. Left: associatively activated processes. Right: dissociatively activated processes.

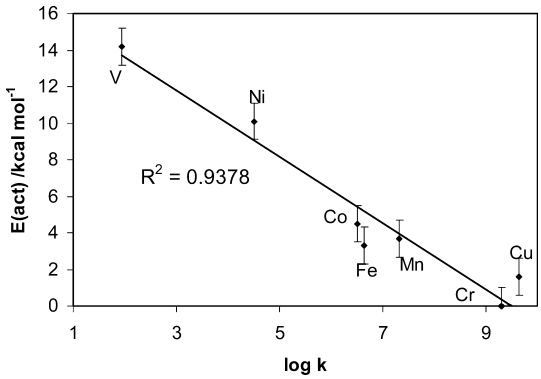

Figure 14. Correlation between log *k* values (and calculated activation energies with the latter showing an estimated uncertainty of ± 1 kcal mol^{-1}.

parameters which alter the calculated bond lengths of the starting complexes by up to, say, 0.04 Å may change the total LFMM energy of that system by up to 6 kcal mol^{-1} but there is significant error cancelation for the activation energies which change by no more than 1 kcal mol^{-1}. However, the parameters are not unique and thus while the overall result is good, the individual contributions to the activation process do not show any discernible trends (Figure 13). However, the conventional connection between the LFSE and Δ_{oct} implicitly assumes that the former is purely an electronic effect while this study and those of Johnson and Nelson[4–7] show that there are more factors involved than just the change in d electron energy. Hence, to make better contact with experiment, both thermodynamic and kinetic, all the factors should be included, and it is the performance of the ensemble rather than any individual component which is significant.

Taking the lowest calculated "activation energy" for each metal (apart from zinc) generates a good correlation with the logarithm of the rate constants (Figure 14) with an R^2 value of 0.94. Thus, the LFMM parameters developed on the basis of the properties of the reactant species provide *in toto* a good description of their subsequent mechanistic properties. Apparently, the TS models, despite their obvious simplicity, are reasonable approximations.

Conclusions

LFMM parameters for the first-row divalent hexaaqua complexes from Cr(II) through to Zn(II) have been designed to reproduce a range of experimental observables including the hydration enthalpy and geometry. In addition to the strong Jahn−Teller distortions for d^4 Cr(II) and d^9 Cu(II), we present the first LFMM calculations of purely π-type Jahn−Teller distortions for d^6 Fe(II) and d^7 Co(II). Although the bond length changes for the iron and cobalt systems are smaller than for chromium and copper, the energy changes relative to the octahedral precursor are comparable because for d^6 and d^7 configurations, π-bonding effects become significant and the system can be stabilized by rotations around the M−O vector.

The FF parameters have then been applied to modeling the water exchange reaction in both associative and dissociative modes. By extending the relatively crude CFT treatment of Basolo and Pearson to a general LFT approach, approximate TS models have been optimized and "activation energies" computed relative to Cr(II). The predictive power of the model has been significantly enhanced over the original and is now on a par with sophisticated quantum mechanical methods, at least for the open-shell systems. Zinc displays a qualitatively different theoretical behavior which requires further investigation. For the remaining complexes, the lowest energy barrier correlates well with log *k* as well as predicting the mechanistic changeover from associative activation for V(II) and Mn(II) to dissociative activation for Fe(II), Co(II), and Ni(II) as suggested by activation volumes. This study thus fully vindicates the original pioneering work of Basolo and Pearson who suggested significant d-electron effects on the mechanism of exchange and substitution processes at octahedral TM centers.

The LFMM parameters further provide a platform for modeling the energetic as well as the structural changes which occur as water ligands are replaced by other donors. The fact that a parameter set essentially based on ground-state properties also provides a good *qualitative* description of reaction mechanism is an encouraging feature, and we are presently exploring whether a more quantitative treatment of water exchange is possible. Clearly, there are some issues to be resolved such as the negative

activation energies for the chromium species and the problems locating a stable model system for the dissociative pathway for Zn. Moreover, if we really wish to compete with quantum chemistry, we will need to consider other possible pathways and develop procedures for locating true transition states rather than relying on simplified models as was done here. Hopefully, these issues can be addressed via further refinement of the LFMM parameters, perhaps using more automated optimization techniques, and the implementation of methods for locating true saddle points on the potential energy surface.

Acknowledgment. The authors are grateful to Chemical Computing Group and the EPSRC's Chemical Database Service for access to the Cambridge Structural Database. K.R. acknowledges the financial support of the EPSRC.

IC800628J